Chemical and Process Engineering: New Frontiers, 2026, 47(1), e123
DOI: 10.24425/cpe.2026.158121

Ultrasound-assisted direct exfoliation using supercritical carbon dioxide as a novel method of graphene flake production

Małgorzata Djas[1,2*], Jakub Jagiełło[2], Artur Dobrowolski[2], Magdalena Romaniec[2], Marek Henczka[1], Krystian Kowiorski[2]

[1] Warsaw University of Technology, Faculty of Chemical and Process Engineering, Waryńskiego 1, 00-645, Warsaw, Poland
[2] Łukasiewicz Research Network – Institute of Microelectronics and Photonics, Aleja Lotników 32/46, 02-668, Warsaw, Poland

*** Corresponding author, e-mail:**
malgorzata.djas@pw.edu.pl

Presented at
XIV Polish Conference
on Multiphase Flows
13–15 September 2025,
Gdańsk, Poland.
Guest Editor:
Donata Konopacka-Łyskawa

Article info:
Received: 14 September 2025
Revised: 11 November 2025
Accepted: 20 January 2026

Abstract
In the present study, a new method involving ultrasound-assisted direct exfoliation with supercritical carbon dioxide is reported for graphene flake production. The influence of the starting material type – graphite (natural and expanded graphite) and duration of ultrasound treatment on the quality of the produced graphene-based material was assessed. By conducting scanning electron microscopy and Raman spectroscopy, it was found that the use of expanded graphite combined with 5 h of sonication in supercritical carbon dioxide yielded graphene nanoplatelets.

Keywords
graphene flake, graphene nanoplatelets, direct exfoliation, supercritical carbon dioxide, ultrasound

1. INTRODUCTION

Graphene, considered one of the most promising materials of the 21st century, has largely transformed the fields of science and technology. This two-dimensional material, isolated by Andre Geim and Konstantin Novoselov in 2004, has been rapidly recognized as a "wonder material" because of its unique properties (Novoselov et al., 2004). Graphene consists of a single layer of carbon atoms with sp^2 hybridization, arranged in a hexagonal structure. This specific arrangement of atoms renders graphene its distinct characteristics, namely high thermal conductivity (4840–5300 W/(m·K)), high electron mobility ($> 15,000$ cm^2/(V·s)), large specific surface area (2630 m^2/g), high mechanical strength (130 GPa), and impermeability to gases (Lee et al., 2008; Magaña et al., 2016). Although the initial excitement surrounding this material remains to be translated into a technological revolution, graphene continues to attract the interest of researchers and is extensively studied for production methods and practical applications. Currently, research is being conducted on the application of graphene in electronics, medicine, next-generation batteries, sensors, lubricants, composite materials, and protective coatings (Djas et al., 2022; Kowiorski et al., 2023; Krawczyk et al., 2025; Worku and Ayele, 2023). Because graphene has a wide range of potential commercial applications, intensive efforts are being made to develop efficient and environmentally friendly production methods.

Besides layered (epitaxial) graphene, flake graphene is one of the primary forms of graphene and is obtained by top-down methods that separate carbon layers in graphite into individual graphene sheets. The most commonly used methods for producing graphene flakes are the oxidation–reduction process and the direct exfoliation of graphite (Hutapea et al., 2025; Zhang et al., 2025). In the oxidation–reduction method, graphite flake is oxidized to introduce oxygen groups between the carbon layers, thereby increasing interlayer distance and weakening interactions (intercalation). The oxidation process is conducted using concentrated acids, such as H_2SO_4, in the presence of strong oxidizers (e.g., $KMnO_4$). The subsequent steps include exfoliation of graphite oxide into graphene oxide, reduction to eliminate oxygen functional groups, and purification and drying of the material. Direct exfoliation of graphite to produce graphene involves in the classical approach the use of organic solvents such as ethanol, 2–propanol, N,N–dimethylformamide, or N–methyl–2–pyrrolidone. The resulting suspension is then treated with ultrasound to achieve exfoliation (Du et al., 2013; Xu et al., 2018).

However, these classical methods of graphene flake production have several limitations. Although the oxidation–reduction method is relatively economical and yields high amounts of material, the obtained graphene is of low quality due to numerous structural defects caused by oxygen functional groups. Moreover, the production process involves hazardous and toxic chemicals (concentrated acids, strong oxidizers, and

reducing agents), which generates a large amount of harmful wastewater, leading to environmental threat. Additionally, the process is multistage and time-consuming and requires costly purification of the final product. Moreover, the main disadvantage of direct exfoliation is the use of volatile organic solvents, which cause harmful effects on human health and the environment and therefore should be avoided. Furthermore, prolonged sonication and subsequent purification from solvent residues are necessary, which increases production costs. The advantage of direct exfoliation, however, is that the resulting graphene is less defective and therefore exhibits different properties compared to graphene oxide or reduced graphene oxide. Hence, there is a strong need to develop methods for producing high-quality and pure graphene while ensuring high yield, short processing time, and environmental safety. Thus, the rapid development of new graphene production technologies requires the implementation of sustainable development strategies and the principles of Green Chemistry in industrial practice.

An effective and environmentally friendly method to produce graphene flakes is direct exfoliation using supercritical carbon dioxide ($scCO_2$). In this process, graphite – composed of many stacked carbon layers – serves as the starting material. The graphite layers are separated into single graphene sheets in the presence of $scCO_2$. This process can be divided into three stages: (1) pretreatment of graphite (e.g., expansion), (2) intercalation of graphite with CO_2 molecules, and (3) exfoliation (peeling off) (Fig. 1). In stage 1, graphite undergoes expansion, i.e., thermal treatment, to widen interlayer spacing and facilitate CO_2 penetration during intercalation in stage 2. Exfoliation (stage 3) is achieved through rapid depressurization, during which $scCO_2$ transitions to the gaseous state and substantially increases its volume. This stage can be further enhanced by shear stress generation or ultrasonic treatment (Gai et al., 2018; Gao et al., 2017). Thus, in this method, $scCO_2$ acts as a solvent, an intercalating agent that penetrates between graphite layers, and a separating agent during depressurization.

Supercritical fluids possess unique physicochemical properties, which are intermediate between those of liquids and gases. Because of their low surface tension, excellent wettability, and high diffusion coefficient, supercritical fluids are particularly suitable for direct exfoliation processes. Direct exfoliation with $scCO_2$ is a rapid, single-step method to produce graphene flakes. It eliminates the use of hazardous organic solvents utilized in the classical direct exfoliation method. As $scCO_2$ converts into gas upon decompression, the obtained graphene is pure and contains fewer defects; thus, it shows superior electrical conductivity compared to graphene produced by other methods. However, the material produced by direct exfoliation in $scCO_2$ assisted with US has more than a few carbon layers compared to graphene oxide (1–3 layers) produced using oxidation-reduction process and has relatively small size of flakes due to the destructive effects of ultrasound.

Direct exfoliation in $scCO_2$ is a relatively new and scarcely studied approach for graphene flake production. To date, only a few studies have explored this method. This method was first reported in 2009 (Pu et al., 2009), where natural graphite was used as the starting material, and exfoliation was conducted in a reactor at 45 °C and 10 MPa for 30 min, followed by rapid depressurization. The material released with CO_2 was transferred into a vessel containing sodium dodecyl sulfate (SDS) to prevent reaggregation. The obtained graphene had approximately 10 layers, and nearly 30–40% of the graphite was exfoliated. However, CO_2 diffusion between graphite layers is relatively slow, requiring a long processing time and yielding unsatisfactory results. To enhance exfoliation and improve efficiency, additional techniques such as compression–decompression cycles, stirring, shear stress generation, or ultrasound can be applied (Gao and Hu, 2016). For example, graphene nanosheets were obtained by exfoliating expanded graphite in $scCO_2$ combined with repeated compression–decompression cycles, which improved yield and reduced flake thickness (Sim et al., 2012). Li et al. (2016) applied intensive stirring during exfoliation of expanded graphite in $scCO_2$ which enhanced material quality, with 90% of the obtained graphene nanosheets containing fewer than 10 layers.

In 2014, Wang et al. (2014) reported the first study involving the combined utilization of $scCO_2$ and ultrasound for exfoliation. Natural graphite was exfoliated at 40 °C and 8 MPa for 30 min, with an ultrasound power of 60 to 300 W. Subsequently, the mixture was depressurized, and the material released with CO_2 was collected in ethanol and centrifuged (1500 rpm, 60 min). The supernatant alone was analyzed by atomic force microscopy (AFM), transmission electron microscopy (TEM), and Raman spectroscopy. The results showed that ultrasound improved the quality of the exfoliated material, and a higher ultrasound power enhanced the charac-

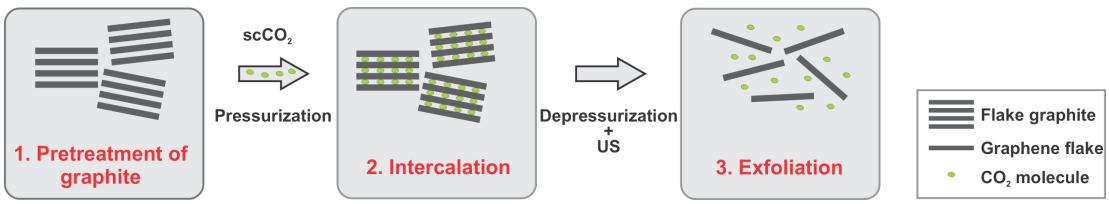

Figure 1. Schematic of graphene flake production through direct exfoliation with $scCO_2$.

teristics of the graphene product. AFM analysis confirmed that increasing ultrasound power reduced flake thickness: at 60 W, the material comprised 4–10 layers; at 120 W, a two-layer graphene product was obtained; and at 300 W, a monolayer graphene product was achieved (Wang et al., 2014). Gao et al. (2014) demonstrated that process parameters such as sonication time, ultrasound power, and pressure significantly influence exfoliation efficiency in $scCO_2$. By using natural graphite (0.2–2.0 g) as the starting material, exfoliation was conducted at 40 °C under 8–18 MPa pressure. The sonication time ranged from 15 to 120 min, and ultrasound power varied from 12 to 240 W. Following exfoliation, the system was depressurized, and the released material was collected in ethanol and centrifuged for 30 min. The best-quality material was obtained under the following conditions: 0.5 g graphite, 12 MPa, 120 W, and 60 min. It was observed that 94% of the material contained fewer than three layers, with 24% being monolayer, 44% bilayer, and 26% trilayer graphene (Gao et al., 2014).

In the present study, for the first time, we report comparative experimental results on the production of graphene flakes by direct exfoliation with $scCO_2$ and $scCO_2$ combined with ultrasound. Moreover, ultrasound-assisted exfoliation was conducted using two types of starting materials: natural graphite and expanded graphite prepared from it. Previous studies have used only a single form of graphite and did not examine the influence of the raw material on process efficiency. Furthermore, unlike earlier reports, the entire obtained material was analyzed in the present study, rather than only the fraction of the thinnest graphene collected after centrifugation.

2. MATERIALS AND METHODS

For graphene production by direct exfoliation, two types of graphite were utilized: natural graphite N1 (Asbury 1 Flake, Asbury Carbons, USA; flake size 180–425 μm) and expanded graphite E1. Expanded graphite E1 was produced from natural graphite N1 by using a proprietary modification and expansion method developed at the Łukasiewicz Research Network – Institute of Microelectronics and Photonics. A mixture of concentrated sulfuric acid and nitric acid was added to natural graphite N1 and then stirred. The intercalated graphite was separated from the acid mixture, washed with water, and the resulting precipitate was dried (100 °C, 90 min). The dry material was then expanded by rapidly heating it in a furnace to 1050 °C for 2 min. Figure 2 shows a schematic of the experimental setup for direct exfoliation of graphite with $scCO_2$.

The main component was a high pressure reactor with a volume of 250 cm^3 (Parr Instrument Company, USA; 34 MPa, 500 °C), equipped with a sonotrode and ultrasonic generator (Hielscher Ultrasonics GmbH, Germany; 26 kHz, maximum generator's power: 200 W). A 0.5 g sample of graphite was placed in the reactor. Liquid CO_2 (Linde, Poland; purity $>$ 99.9996%) was then introduced into the reactor by using a pump equipped with a cooling module (SFT-25, Supercritical Fluid Technologies, USA; 68.9 MPa, 125 cm^3/min). The reactor contents were stabilized at 35 °C and 15 MPa, and sonication was then initiated. The operating parameter of the generator was set to a constant amplitude of 80% of the maximum amplitude (135 μm). Ultrasonic treatment was performed in 8-min cycles consisting of 5 min of sonication at 3-min intervals. The experiments were conducted for different total processing times, including pauses: 1.5, 3, and 5 h. Following process completion, the system was rapidly depressurized by quickly opening the outlet valve. The powder remaining in the reactor was characterized by scanning electron microscopy (SEM) and Raman spectroscopy. Selected exfoliated samples were centrifuged with isopropyl alcohol (4000 rpm and 30 min), and the fraction present in the supernatant was analyzed by SEM and Raman spectroscopy. Exfoliation experiments using only $scCO_2$ were conducted using the same setup, but with the ultrasonic generator switched off. After 5 h of graphite intercalation with CO_2, the reactor contents were rapidly depressurized.

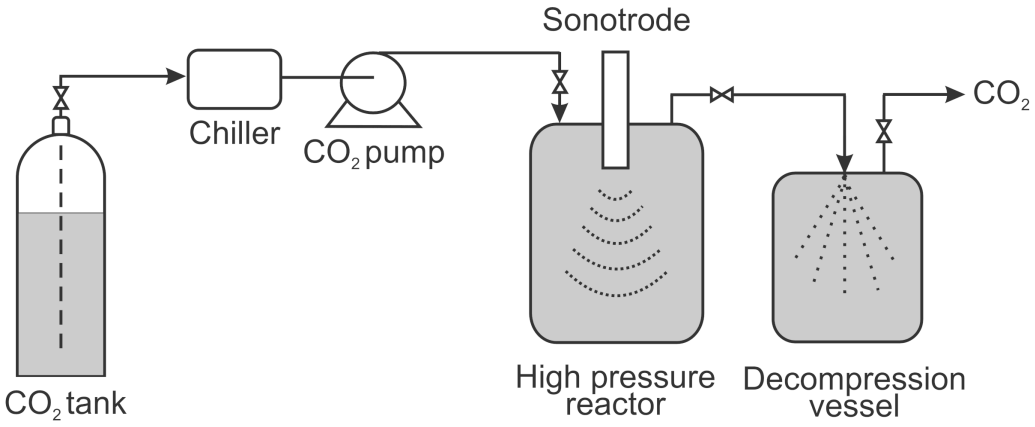

Figure 2. Schematic of the experimental setup.

2.1. Scanning electron microscopy

SEM was performed using a field-emission scanning electron microscope (FE-SEM, Auriga® CrossBeam® Workstation, Carl Zeiss, Oberkochen, Germany). Samples were mounted on carbon tape prior to measurements. The microscope was equipped with an Everhart–Thornley detector (SE2), an In-lens detector, and an energy selective backscattered (EsB) detector. Secondary electron (SE) and backscattered electron (BSE) signals were acquired at 1 or 5 kV accelerating voltage and 3–5.5 mm working distance.

2.2. Raman spectroscopy

Room-temperature Raman spectra were acquired using a Renishaw InVia Raman spectrometer (Renishaw, United Kingdom) equipped with the 532 nm (2.33 eV) line of an Nd:YAG laser and a Renishaw detector. The laser beam was focused on the sample surface through a 100× objective lens, with the laser power maintained at 1 mW. To improve statistical accuracy, 1000-point Raman maps were collected. The spectra were analyzed using Renishaw's WiRE software. The data analysis methodology was based on the acquisition of a large number of Raman spectra across the investigated area, which were subsequently integrated into an averaged spectrum. Such an approach provides rigorous control over the peak-fitting procedure, as it confines the analysis to a single representative spectrum while preserving the statistical significance of the dataset. This approach minimizes local spectral variability, reduces random noise contributions, and improves the accuracy and reproducibility of material-to-material comparisons.

In graphite Raman spectra, the 2D mode typically exhibits a two-peak profile: a more intense $2D_1$ mode and a lower-energy shoulder, $2D_2$, resulting from interactions between adjacent graphitic planes (Kaniyoor and Ramaprabhu, 2012). In the present study, the intensity ratio of the $2D_1$ and $2D_2$ modes ($I2D_1/I2D_2$) was analyzed. With increasing disorder, the $2D_2$ peak shifts upward and eventually merges with the $2D_1$ mode. Consequently, the 2D band evolves into a single-peak profile, indicating the loss of three-dimensional ordering.

3. RESULTS AND DISCUSSION

Figure 3 shows SEM images of natural graphite (N1) and expanded graphite (E1) derived from natural graphite, which were used as the starting materials for exfoliation in $scCO_2$. Natural graphite occurs as flakes containing many closely packed carbon layers. In contrast, expanded graphite, obtained by treating natural graphite, comprises long ribbons formed due to the separation of carbon layers during high-temperature expansion. The carbon layers, which are tightly stacked in natural graphite, are considerably separated in expanded graphite. This increased interlayer spacing may enhance the efficiency of graphite exfoliation by facilitating the penetration of CO_2 molecules between the layers and increasing the surface area available for ultrasonic interaction.

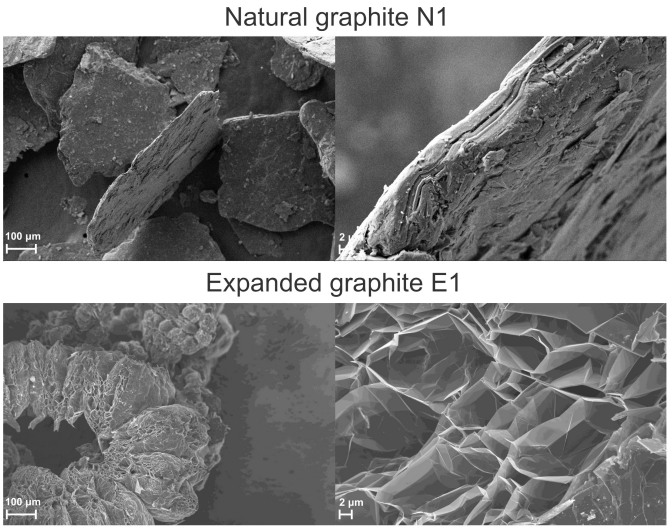

Figure 3. SEM images of natural graphite and expanded graphite.

Figures 4 and 5 show SEM images of carbon materials obtained from ultrasound-assisted exfoliation of natural and expanded graphite in $scCO_2$. For comparison, Figure 5 also shows SEM images of materials obtained from expanded graphite after exfoliation in $scCO_2$ without ultrasound assistance (sample E1–5h).

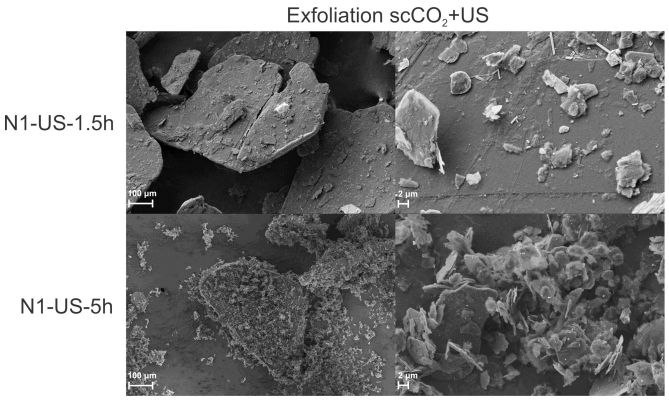

Figure 4. SEM images of carbon materials obtained from natural graphite (N1) by ultrasound-assisted direct exfoliation in $scCO_2$ ($scCO_2$+US).

First, exfoliation in $scCO_2$ without ultrasound assistance was tested using expanded graphite, which is more prone to exfoliation than natural graphite. A relatively long intercalation time of 5 h was applied, followed by exfoliation performed through rapid depressurization of the reactor (sample E1–5h). As observed in SEM images (Fig. 5), the morphology of the resulting material closely resembles that of the starting expanded graphite. Graphite ribbons remain visible, and the carbon layers appear largely intact. This observation suggests that exfoliation in $scCO_2$ with rapid decompression alone is not an efficient method to produce graphene-based material. Moreover, extended CO_2 intercalation and sudden decompression proved insufficient to generate graphene. Therefore, to improve the exfoliation process, ultrasound was introduced in $scCO_2$.

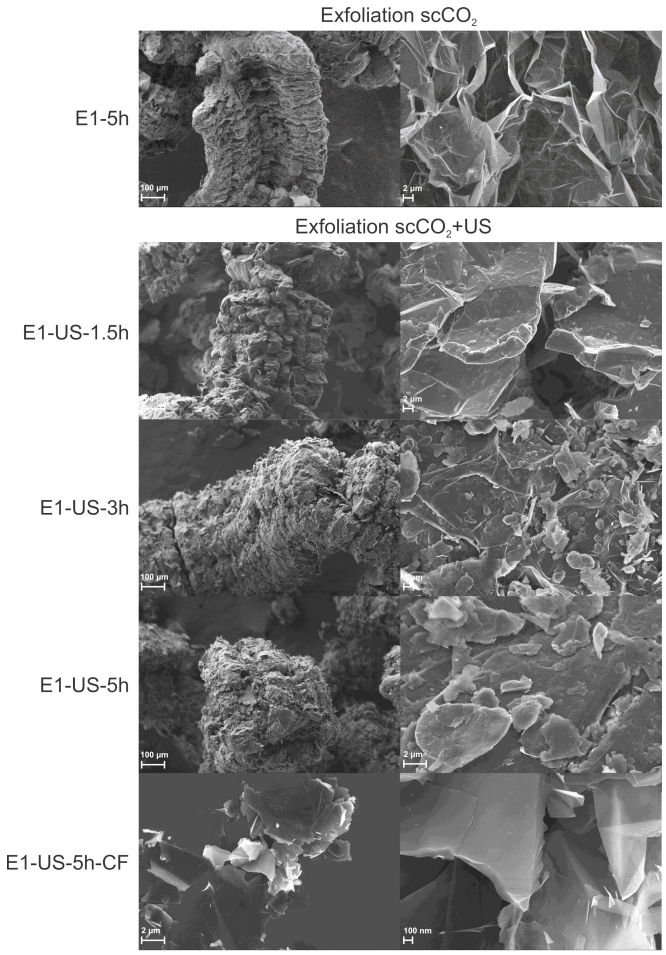

Figure 5. SEM images of carbon materials obtained from expanded graphite (E1) by direct exfoliation in $scCO_2$ and ultrasound-assisted direct exfoliation in $scCO_2$ ($scCO_2$+US).

Figures 4 and 5 show SEM images of the materials obtained after ultrasound-assisted exfoliation in $scCO_2$. When natural graphite was used as the feedstock (Fig. 4), ultrasonic treatment combined with $scCO_2$ for 1.5 h produced no significant morphological changes (N1-US-1.5h). However, extending the process to 5 h caused material fragmentation (N1-US-5h). SEM images of sample N1-US-5h revealed numerous small flakes detached from larger ones, although large unexfoliated graphite flakes remained. Because this method showed low efficiency with natural graphite, expanded graphite was used as the feedstock in subsequent experiments. Figure 5 shows SEM images of the resulting materials.

Exfoliation of expanded graphite for 1.5 h (sample E1-US-1.5h) produced no major changes compared to the starting material (Fig. 3), as graphite ribbons remained visible. Following 3 h of exfoliation (E1-US-3h, Fig. 5), the surface of the graphite ribbons appeared frayed, and this effect was more prominent after 5 h (E1-US-5h). Higher magnification SEM images of the materials from the 3 h and 5 h processes revealed highly frayed structures and detached smaller, thinner flakes. This morphology indicates significant heterogeneity, with the presence of both thin graphene-like flakes and thicker graphite flakes. However, in the 5 h sample, thin graphene flakes predominated, although a few thick, unexfoliated flakes were still observed. Thus, the SEM results suggest that the material obtained after 5 h exfoliation contained graphene nanoplatelets (GNPs). The lateral size of the flakes in the obtained material (E1-US-5h) is in the range of 1.0–8.7 µm.

The material obtained after 5 h of ultrasound-assisted exfoliation was further centrifuged to isolate the thinnest flakes (sample E1-US-5h-CF). SEM images (Fig. 5) show isolated thin graphene flakes (flake lateral size in the range of 540.1 nm–7.9 µm) without residual graphite flakes, demonstrating effective graphite delamination into graphene layers and high material homogeneity.

Figure 6 shows the averaged Raman spectra and Table 1 presents the Raman analysis results for the investigated samples, i.e., natural and expanded graphite as well as exfoliated materials obtained following $scCO_2$ and ultrasound treatment.

According to the Raman spectra of natural graphite, ultrasound-assisted exfoliation in $scCO_2$ reduced the $I2D_1/I2D_2$ ratio compared to that of pristine graphite (1.20 → 1.03). However, extending the exfoliation time from 1.5 h to 5 h had no further change on this ratio. For expanded graphite (Fig. 6, Table 1), increasing the sonication time in $scCO_2$ to 5 h steadily decreased the $I2D_1/I2D_2$ ratios (1.60 → 1.38 → 1.28 → 0.97), indicating progressively thinner

Table 1. Raman fitting parameters of materials obtained by ultrasound-assisted exfoliation in $scCO_2$.

Sample	$2D_1$ position [cm^{-1}]	FWHM $2D_1$ [cm^{-1}]	$2D_2$ position [cm^{-1}]	FWHM $2D_2$ [cm^{-1}]	ID/IG	$I2D_1/I2D_2$	ID/ID'
N1	2722.8	42.6	2685.5	58.1	0.10	1.20	5.0
N1-US-1.5h	2720.1	42.8	2683.1	61.0	0.28	1.03	3.4
N1-US-5h	2718.5	43.2	2681.8	63.6	0.20	1.03	3.2
E1	2723.3	40.5	2684.7	50.8	–	1.60	–
E1-US-1.5h	2722.3	43.5	2685.1	55.1	0.08	1.38	4.0
E1-US-3h	2722.3	42.5	2684.9	56.4	0.20	1.28	3.2
E1-US-5h	2721.5	37.4	2687.8	61.4	0.17	0.97	3.6
E1-US-5h-CF	2718.9	42.6	2684.9	62.7	0.24	0.84	2.8

material formation. An $I2D_1/I2D_2$ ratio of 0.97 for the 5 h sample suggests the loss of three-dimensional ordering (Kaniyoor and Ramaprabhu, 2012). After centrifugation, the E1-US-5h-CF sample showed a further reduced ratio of 0.84, confirming that it had more graphene-like nature compared to the non-centrifuged 5 h sample. This is consistent with our expectations, as centrifugation was intended to isolate the thinnest graphene fractions. These Raman results corroborate the SEM observations.

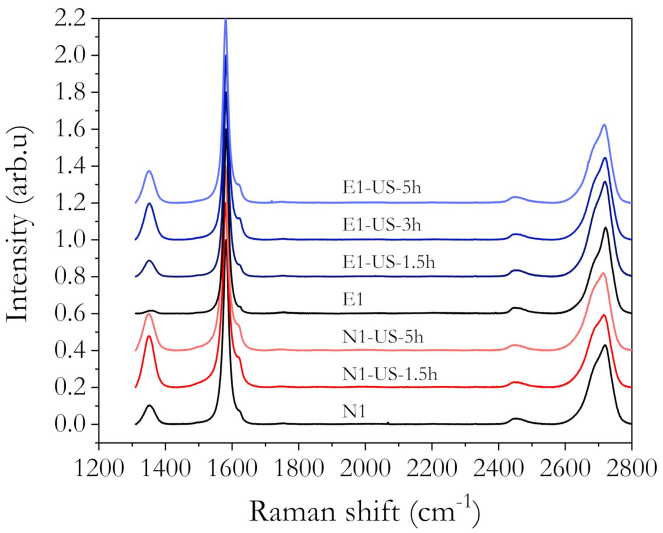

Figure 6. Raman spectra of natural and expanded graphite and of materials obtained by ultrasound-assisted exfoliation in $scCO_2$.

Figure 7 compares the Raman spectrum of E1 graphite with the single spectra from the Raman maps of samples E1-US-5h and E1-US-5h-CF. Compared to the asymmetric 2D peak of graphite, the symmetric 2D peak of the E1-US-5h sample indicates the formation of GNPs. GNPs are thin stacks of graphene layers with thickness from 5 nm to 60–100 nm (15–300 carbon layers) (Fatima et al., 2017; Prolongo et al., 2014; Shen et. al., 2021). The symmetry and lack of splitting of the 2D peak facilitate I2D/IG analysis, which provides an estimate of the number of graphene layers. For the 5 h sample, the I2D/IG ratio was 0.34, consistent with a few-layer graphene-based material (Abas et al., 2022), compared to ~ 2 for single-layer graphene (Ferrari, 2007). The spectrum of sample E1-US-5h-CF also shows a symmetric 2D peak, with an increased I2D/IG ratio of 0.42, suggesting thinner nanoplatelets than those in the non-centrifuged E1-US-5h sample.

As expected, in the expanded graphite-based samples, the $2D_2$ peak shifted toward higher wavenumbers as exfoliation time increased (Table 1). This occurred because of the loss of three-dimensionality and increased graphene-like characteristics of the material, corresponding to the formation of a single 2D mode. Simultaneously, the $2D_1$ peak shifted to lower wavenumbers. The full width at half maximum (FWHM) increased for $2D_2$ and decreased for $2D_1$ during exfoliation.

The ID/IG ratio represents the level of defects in the material (Cançado et al., 2011). For graphite, the D band intensity is

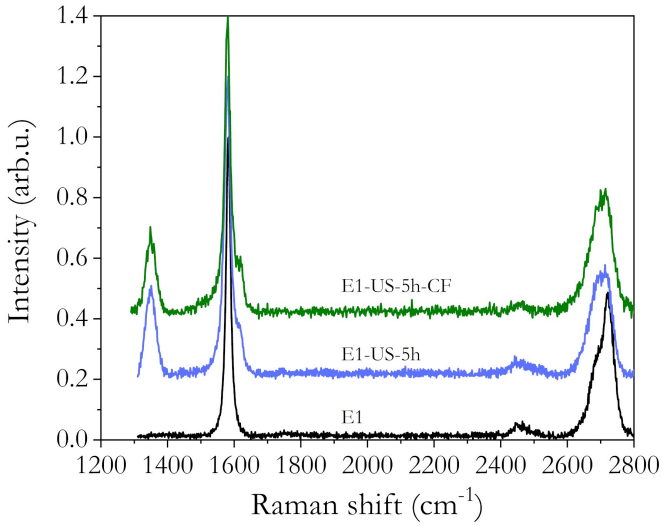

Figure 7. Raman spectra of expanded graphite and materials obtained after 5 h of ultrasound-assisted exfoliation in $scCO_2$.

very low because its 3D structure is intact. However, during exfoliation and thinning, the D band intensity increased. For the 5 h exfoliated sample, the ID/IG ratio was 0.17, which corresponds to very low defect density compared to that in other graphene-based materials. For example, reduced graphene oxide typically exhibits an ID/IG ratio of 1.0–1.9 (Das et al., 2021; Silva Filho et al., 2020).

The ID/ID' ratio enables to identify the defect type (Eckmann et al., 2012). For all samples sonicated in $scCO_2$, the ID/ID' ratio was approximately 3.5, indicating that edge defects were predominant. This is consistent with material thinning and the corresponding increase in the edge-to-surface ratio of the flakes.

4. CONCLUSIONS

The results of the present study confirm that ultrasound-assisted exfoliation in $scCO_2$ is a highly efficient method to produce GNPs. Graphite intercalation with $scCO_2$ followed by rapid depressurization alone is insufficient to obtain graphene-based materials with superior quality. However, the combination of ultrasound and $scCO_2$ substantially enhances the efficiency of the exfoliation method and the quality of the obtained product.

The performance of the investigated method depends on the type of graphite used as the feedstock and ultrasonic treatment duration. Expanded graphite treated with the longest sonication time (5 h) yielded multilayer GNPs. This is because the separated carbon layers in expanded graphite after pretreatment facilitate CO_2 penetration and effective delamination. Prolonged sonication in $scCO_2$ produces materials with increasingly graphene-like characteristics. In contrast, natural graphite with its tightly packed carbon layers shows considerably lower exfoliation efficiency in $scCO_2$, and extending the process time does not improve material quality.

GNPs obtained after 5 h of sonication showed high quality with low defect density, dominated by edge-type defects. Prolonged sonication in $scCO_2$ not only enables effective delamination of expanded graphite but also induces flake fragmentation and size reduction. The resulting graphene-based material showed moderate heterogeneity, with flakes of varying thickness and a small fraction of graphite residues. To address this limitation, further optimization of graphite selection, preparation, and process parameters is required. Although material homogeneity can be improved by fractionation (e.g., centrifugation), this approach is impractical for industrial applications and diminishes the advantages of $scCO_2$-based exfoliation, as it requires the use of organic solvents and drying steps, which further reduces process efficiency.

Ultrasound-assisted exfoliation in $scCO_2$ is a rapid, simple, and environmentally friendly method to produce GNPs. Because of these advantages, it has potential for application in industrial-scale GNP production. Currently, GNPs are being widely applied in many fields such as nanocomposites for automotive and aerospace industries, 3D printing, lubricants, conductive pastes, and electronics (Khan et al., 2024; Yee and Ghayesh, 2023). This wide application potential of GNPs justifies the continued development of $scCO_2$-based exfoliation methods.

ACKNOWLEDGMENTS

This research was funded by the National Science Centre, Poland – grant "Identification of mechanisms and investigations of flake graphene production by direct exfoliation using supercritical carbon dioxide", project number 2019/35/D/ST8/02977.

This research was funded by the National Centre for Research and Development, Poland, under Grant Agreement No. M-ERA.NET3/2021/83/I4BAGS/2022. The M-ERA.NET3 has received funding from the European Union's Horizon 2020 research and innovation programme under Grant Agreement No. 958174.

REFERENCES

Abas A.F., Lau K.Y., Muhammad F.D., Abdulkawi W.M., Al-Moliki Y.M., Alresheedi M.T., Mahdi M.A., 2022. Dual-wavelength mode-locked oscillation with graphene nanoplatelet saturable absorber in erbium-doped fiber laser. *Electronics*, 11, 2880. DOI: 10.3390/electronics11182880.

Cançado L.G., Jorio A., Martins Ferreira E.H., Stavale F., Achete C.A., Capaz R.B., Moutinho M.V.O., Lombardo A., Kulmala T.S., Ferrari A.C., 2011. Quantifying defects in graphene via raman spectroscopy at different excitation energies. *Nano Lett.*, 11, 3190–3196. DOI: 10.1021/nl201432g.

Das P., Deoghare A.B., Maity S.R., 2021. A novel approach to synthesize Reduced Graphene Oxide (RGO) at low thermal conditions. *Arab. J. Sci. Eng.*, 46, 5467–5475. DOI: 10.1007/s13369-020-04956-y.

Djas M., Matuszewska A., Borowa B., Kowiorski K., Wieczorek P., Małek M., Chlanda A., 2022. Flake graphene as an innovative additive to grease with improved tribological properties. *Materials*, 15, 7775. DOI: 10.3390/ma15217775.

Du W., Jiang X., Zhu L., 2013. From graphite to graphene: direct liquid-phase exfoliation of graphite to produce single and few-layered pristine graphene. *J. Mater. Chem. A*, 1, 10592–10606. DOI: 10.1039/C3TA12212C.

Eckmann A., Felten A., Mishchenko A., Britnell L., Krupke R., Novoselov K.S., Casiraghi C., 2012. Probing the nature of defects in graphene by Raman spectroscopy. *Nano Lett.*, 12, 3925–3930. DOI: 10.1021/nl300901a.

Fatima S., Ali S.I., Iqbal M.Z., Rizwan S., 2017. The high photocatalytic activity and reduced band gap energy of La and Mn co-doped $BiFeO_3$/ graphene nanoplatelet (GNP) nanohybrids. *RSC Adv.*, 7, 35928–35937. DOI: 10.1039/c7ra04281g.

Ferrari A.C., 2007. Raman spectroscopy of graphene and graphite: disorder, electron–phonon coupling, doping and nonadiabatic effects. *Solid State Commun.*, 143, 47–57. DOI: 10.1016/j.ssc.2007.03.052.

Gai Y., Wang W., Xiao D., Zhao Y., 2018. Ultrasound coupled with supercritical carbon dioxide for exfoliation of graphene: simulation and experiment. *Ultrason. Sonochem.*, 41, 181–188. DOI: 10.1016/j.ultsonch.2017.09.007.

Gao H., Hu G., 2016. Graphene production *via* supercritical fluids. *RSC Adv.*, 6, 10132–10143. DOI: 10.1039/C5RA15568A.

Gao Y., Shi W., Wang W., Wang Y., Zhao Y., Lei Z., Miao R., 2014. Ultrasonic-assisted production of graphene with high yield in supercritical CO_2 and its high electrical conductivity film. *Ind. Eng. Chem. Res.*, 53, 2839–2845. DOI: 10.1021/ie402889s.

Gao H., Zhu K., Hu G., Xue C., 2017. Large-scale graphene production by ultrasound-assisted exfoliation of natural graphite in supercritical CO_2/H_2O medium. *Chem. Eng. J.*, 308, 872–879. DOI: 10.1016/j.cej.2016.09.132.

Hutapea J.A.A., Manik Y.G.O., Ndruru S.T.C.L., Huang J., Goei R., Tok A.I.Y., Siburian R., 2025. Comprehensive review of graphene synthesis techniques: advancements, challenges, and future directions. *Micro*, 5, 40. DOI: 10.3390/micro5030040.

Kaniyoor A., Ramaprabhu S., 2012. A Raman spectroscopic investigation of graphite oxide derived graphene. *AIP Adv.*, 2, 032183. DOI: 10.1063/1.4756995.

Khan S.A., Ghazi S.M.U., Amjad H., Imran M., Khushnood R.A., 2024. Emerging horizons in 3D printed cement-based materials with nanomaterial integration: a review. *Constr. Build. Mater.*, 411, 134815. DOI: 10.1016/j.conbuildmat.2023.134815.

Kowiorski K., Heljak M., Strojny-Nędza A., Bucholc B., Chmielewski M, Djas M., Kaszyca K., Zybała R., Małek M., Swieszkowski W., Chlanda A., 2023. Compositing graphene oxide with carbon fibers enables improved dynamical thermomechanical behavior of papers produced at a large scale. *Carbon*, 206, 26–36. DOI: 10.1016/j.carbon.2023.02.009.

Krawczyk J., Korec-Kosturek J., Kosturek R., Jakubowska I., Pakuła A. Djas M., Kowiorski K., Stasiewicz K.A., 2025. Use of graphene oxide as an active layer on a tapered fibre for detection of volatile liquid vapours: ammonium hydroxide, trimethyl phosphate, and 1,4-thioxane. *Opto-Electron. Rev.*, 33, e154305. DOI: 10.24425/opelre.2025.154305.

Lee C., Wei X., Kysar J.W., Hone J., 2008. Measurement of the elastic properties and intrinsic strength of monolayer graphene. *Science*, 321, 385–388. DOI: 10.1126/science.1157996.

Li L., Xu J., Li G., Jia X., Li Y., Yang F., Zhang L., Xu C., Gao J., Liu Y., Fang Z., 2016. Preparation of graphene nanosheets by shear-assisted supercritical CO_2 exfoliation. *Chem. Eng. J.*, 284, 78–84. DOI: 10.1016/j.cej.2015.08.077.

Magaña R.V., Barriga-Arceo L.D., Palacios E., Vázquez G.L.R., Garibay-Febles V., Morales R.D., Martinez-Reyes J., 2016. Exfoliation of graphite with yttrium oxide via mechanical alloying and irradiation with microwaves, In: Aliofkhazraei M., Ali N., Milne W.I., Ozkan C.S., Mitura S., Gervasoni J.L. (Eds.), *Graphene Science Handbook: Fabrication Methods*. CRC Press Taylor & Francis Group, 385–402. DOI: 10.1201/b19606.

Novoselov K.S., Geim A.K., Morozov S.V., Jiang D., Zhang Y., Dubonos S.V., Grigorieva I.V., Firsov A.A., 2004. Electric field effect in atomically thin carbon films. *Science*, 306, 666–669. DOI: 10.1126/science.1102896.

Prolongo S.G., Jiménez-Suárez A., Moriche R., Ureña A., 2014. Graphene nanoplatelets thickness and lateral size influence on the morphology and behavior of epoxy composites. *Eur. Polym. J.*, 53, 292–301. DOI: 10.1016/j.eurpolymj.2014.01.019.

Pu N.-W., Wang C.-A., Sung Y., Liu Y.-M., Ger M.-D., 2009. Production of few-layer graphene by supercritical CO_2 exfoliation of graphite. *Mater. Lett.*, 63, 1987–1989. DOI: 10.1016/j.matlet.2009.06.031.

Shen M.-Y., Liao W.-Y., Wang T.-Q., Lai W.-M., 2021. Characteristics and mechanical properties of graphene nanoplatelets-reinforced epoxy nanocomposites: comparison of different dispersal mechanisms. *Sustainability*, 13, 1788. DDOI: 10.3390/su13041788.

Silva Filho J.C., Venancio E.C., Silva S.C., Takiishi H., Martinez L.G., Antunes R.A., 2020. A thermal method for obtention of 2 to 3 reduced graphene oxide layers from graphene oxide. *SN Appl. Sci.*, 2, 1450. DOI: 10.1007/s42452-020-03241-9.

Sim H.S., Kim T.A., Lee K.H., Park M., 2012. Preparation of graphene nanosheets through repeated supercritical carbon dioxide process. *Mater. Lett.*, 89, 343–346. DOI: 10.1016/j.matlet.2012.08.104.

Wang W., Wang Y., Gao Y., Zhao Y., 2014. Control of number of graphene layers using ultrasound in supercritical CO_2 and their application in lithium-ion batteries. *J. Supercrit. Fluids*, 85, 95–101. DOI: 10.1016/j.supflu.2013.11.005.

Worku A.K., Ayele D.W., 2023. Recent advances of graphene-based materials for emerging technologies. Results Chem., 5, 100971. DOI: 10.1016/j.rechem.2023.100971.

Xu Y., Cao H., Xue Y., Li B., Cai W., 2018. Liquid-phase exfoliation of graphene: an overview on exfoliation media, techniques, and challenges. *Nanomater.*, 8, 942. DOI: 10.3390/nano8110942.

Yee K., Ghayesh M.H., 2023. A review on the mechanics of graphene nanoplatelets reinforced structures. *Int. J. Eng. Sci.*, 186, 103831. DOI: 10.1016/j.ijengsci.2023.103831.

Zhang X., Cao S., Wu X., Hu L., 2025. Overview on comparison of four preparation methods and physical properties of graphene. *Nanomater. Nanotechnol.*, 2025(1). DOI: 10.1155/nax2/8865039.